PCCP

PAPER

View Article Online
View Journal | View Issue



Cite this: *Phys. Chem. Chem. Phys.*, 2020, **22**, 19223

# Two-dimensional IR spectroscopy reveals a hidden Fermi resonance band in the azido stretch spectrum of β-azidoalanine†

Jun Young Park,‡[ab] Hyeok-Jun Kwon,‡[b] Saptarsi Mondal,[ab] Hogyu Han,*[b] Kyungwon Kwak*[ab] and Minhaeng Cho*[ab]

Azido stretch modes in a variety of azido-derivatized nonnatural amino acids and nucleotides have been used as a site-specific infrared (IR) probe for monitoring changes in their conformations and local electrostatic environments. The vibrational bands of azide probes are often accompanied by complex line shapes with shoulder peaks, which may arise either from incomplete background subtraction, Fermi resonance, or multiple conformers. The isotope substitution in the infrared probe has thus been introduced to remove Fermi resonances without causing a significant perturbation to the structure. Here, we synthesized and labeled the mid-N atoms of aliphatic azide derivatives with $^{15}N$ to study the effects of isotope labelling on their vibrational properties. The FT-IR spectra of the aliphatic azide with asymmetric lineshape became a single symmetric band upon isotope substitution, which might be an indication of the removal of the hidden Fermi resonance from the system. We also noticed that the 2D-IR spectrum of unlabeled aliphatic azide has cross-peaks, even though it is not apparently identifiable. The 1D slice spectra obtained from the 2D-IR spectra reveal the existence of a hidden Fermi resonance peak. Furthermore, we show that this weak Fermi resonance does not produce discernible oscillatory beating patterns in the IR pump–probe spectrum, which has been used as evidence of the Fermi resonance. Therefore, we confirm that isotope labelling combined with 2D-IR spectroscopy is the most efficient and incisive way to identify the origin of small shoulder peaks in the linear and nonlinear vibrational spectra of various IR probe molecules.

Received 18th May 2020,
Accepted 7th August 2020

DOI: 10.1039/d0cp02693j

rsc.li/pccp



## Introduction

Understanding the conformational changes and dynamics of proteins is vital as they control biological functions and reactions inside cells. Depending on their local environments, proteins could undergo various structural transitions from one conformer to another, which often dictates their biological activities. Therefore, many efforts have been made to elucidate protein conformational changes and dynamics using various spectroscopic techniques.[1,2] Fluorescence spectroscopy has been widely employed to study protein conformational changes and the effects of local environments. In the fluorescence studies, proteins should be labeled with fluorescent proteins or other organic fluorophores.[3,4] Because the fluorescent signal is highly sensitive to subtle biophysical changes in equilibrium or non-equilibrium state, they provide important information on the protein structures and conformational changes. However, the use of fluorophores has one crucial drawback. As typical fluorophores are large in size, they inevitably introduce a perturbation to the native structures of proteins.

Conversely, IR probes, such as carbonyl (CO), nitrile (–CN), thiocyanate (–SCN), and azide ($-N_3$) groups, are relatively small and thereby less perturbative to the native structure when incorporated into amino acids or proteins.[5–8] Furthermore, IR probes are very sensitive to local environments and useful for monitoring conformational changes of proteins. Therefore, over the past two decades, developments of new IR probes which can be attached to specific position in proteins have become an important research area. In particular, the frequency region between 1800–2300 $cm^{-1}$ is referred to as a "transparent window" because solvent water molecules and protein's backbone modes do not absorb IR photons in this frequency range. This transparent

[a] *Center for Molecular Spectroscopy and Dynamics, Institute for Basic Science (IBS), Korea University, Seoul 02841, Republic of Korea. E-mail: kkwak@korea.ac.kr, mcho@korea.ac.kr*

[b] *Department of Chemistry, Korea University, Seoul 02841, Republic of Korea. E-mail: hogyuhan@korea.ac.kr*

† Electronic supplementary information (ESI) available: Characterization for derivatized aliphatic azides; figures and tables showing the IR pump–probe spectra analysis with damped sine function, FT-IR and fitting analysis of derivatized aliphatic azides in water, and anharmonic frequency analysis results. See DOI: 10.1039/d0cp02693j

‡ These authors contributed equally to this work.

window is, therefore, considered an optimal frequency range for linear and nonlinear IR spectroscopic studies of protein structures and dynamics.[9]

Azide IR probes have received special attention because of its large dipole strength. Compared to nitrile stretch modes in various CN–, SCN–, SeCN–, and generally XCN-derivatized compounds, the azido stretch mode has approximately 13 times larger molar extinction coefficient.[8] This strong IR intensity makes the azide group one of the most useful IR probes because minimal use of proteins tagged with IR probes can reduce the cost of sample preparation and more impotantly the probability of protein aggregation. Azide has already been applied to a variety of studies with nonnatural amino acids and proteins as a local IR probe.[10–16] Specifically, azidohomoalanine (AHA) is well-known for being a conformationally sensitive IR probe when introduced into peptides and proteins.[17–19] The frequency of the azide probe in the folded state is quite different from that of the unfolded state due to the sensitivity of vibrational frequency to the local environment; *e.g.*, the azide vibrational frequency in the folded state for NTL9-Met1Aha is 2094 $cm^{-1}$, which is blue-shifted to 2113 $cm^{-1}$ in the unfolded state.[17] However, the frequency shift is often not large enough to make the shifted peak separated from the broad spectrum resulting from multiple conformers. Moreover, the minor or transient conformers do not produce a notable peak in the spectrum due to the small population. As a result, the spectroscopic study of intermediate states or transient conformers requires complex fitting analysis to extract the corresponding spectral signatures from the asymmetric spectrum with one or more weak shoulder peaks. Often, it was necessary to carry out extensive quantum chemistry and vibrational analysis calculations to make the assignment of the hidden peaks convincingly clear.

Ultrafast time-resolved IR spectroscopy is an incisive tool useful for acquiring a molecule-level understanding of the structural and dynamical changes of the protein.[20–29] Femtosecond IR pump–probe and 2D-IR techniques have been successively applied to the investigations of complicated structural dynamics of various proteins in solutions.[30–34] Especially, 2D-IR spectroscopy can enhance the spectral resolution *via* expanding the congested spectrum into a two-dimensional frequency domain, which produces cross-peaks resulting from interactions and chemical or energy exchanges between vibrational modes. In addition, the fourth-order dependence of the signal on the transition dipole moment results in both spectral narrowing and solvent suppression effects, which also enhances the spectral resolution further. These advantages of 2D-IR spectroscopy make it one of the most widely used tools in the investigations of the conformational dynamics of proteins.

Unfortunately, Fermi resonance producing side peaks in the IR probe spectrum limits the use of linear and nonlinear IR spectroscopy with IR probes and makes the interpretation of experimental results difficult. For example, Tucker *et al.* have shown that the multiple transitions in the OCN region of phenyl cyanate originate from the near-resonanct accidental anharmonic couplings between few overtone bands and OCN mode using 2D-IR echo spectroscopy.[35] The azido IR spectrum of an aliphatic β-azidoalanine shows an asymmetric lineshape with shoulder peaks, but their origin has not been elucidated. Okuda *et al.*[36] observed various components in the Fourier-transformed infrared (FT-IR) spectra of Boc-3-azide-Ala-OH ($N_3$-Ala) and *N*-Boc-*cis*-4-azide-L-proline ($N_3$-Pro) salts in water. They assigned the shoulder peak in the $N_3$ region to the peaks originating from multiple conformers. However, the small azido shoulder peak was not detected in their 2D-IR spectra, which raises the question of whether this peak originates from different conformers or Fermi resonance.

Here, we report that the 2D-IR spectroscopy of azido-derivatized alanines provides sufficiently high spectral resolution exhibiting feeble Fermi resonance peak hidden under the broad spectral wing of the FT-IR spectrum. More specifically, the azido stretch peak in the azido-derivatized alanine Ala-$N_3$ (Ac-Ala($N_3$)-NHMe) was studied with 2D-IR, which shows the cross-peak caused by Fermi resonance. On the other hand, Lipkin *et al.* have shown that the $^{15}N$ substitution on the azide is a promising way to remove accidental Fermi resonance.[37] Therefore, we measured the 2D-IR spectra of the $^{15}N$-labeled azide Ala-$N^{15}NN$ (Ac-Ala($N^{15}NN$-NHMe)) to investigate further whether Fermi resonance is reduced because of the isotope substitution at the β position of the azide. Finally, we carried out IR pump–probe measurements to study the effects of isotope labelling on the vibrational relaxation dynamics of the aliphatic azides.

## Experimental methods

### A. Materials

Ala-$N_3$ and Ala-$N^{15}NN$ were synthesized and characterized (ESI).

### B. FT-IR spectroscopy

For FT-IR measurement, we synthesized the labeled and unlabeled compounds as described in the Materials. All azide derivatives were in L form because only L form is active inside a cell. These compounds were used for the following IR pump–probe and 2D-IR experiments. Spectra were measured using a Bruker VERTEX 70 FT-IR spectrometer with a mercury–cadmium–telluride (MCT) detector filled with liquid nitrogen ($N_2$) (Billerica, MA). The frequency resolution of the spectrometer was 1 $cm^{-1}$, and DMF was used as the solvent. All liquid samples were placed in a homemade cell with two $CaF_2$ windows of 2 mm thickness. The path length of the cell was 25 μm using an appropriate Teflon spacer.

### C. IR pump–probe spectroscopy

A Ti:Sapphire oscillator (Tsunami) and regenerative amplifier (Spitfire) (Spectra-Physics, Inc.; Santa Clara, CA) were used to generate an 800 nm pulse with a power of ~1 W. An $AgGaS_2$ crystal was employed to generate a mid-IR pulse with a repetition rate of 1 kHz in an optical parametric amplifier (OPA). The mid-IR pulse was separated by a beam splitter into a pump and probe beam with an intensity ratio of 9 : 1. The time delay was controlled using a motorized linear stage in the probe beamline. Both the pump and probe beam were temporally and spatially

 

overlapped on the sample. The pump–probe signal was dispersed by a monochromator onto a 32-element MCT array detector ($\sim$2 cm$^{-1}$ per pixel resolution). The relative polarization of the probe beam was controlled using a rotating polarizer. To measure isotropic relaxation dynamics, we measured two polarization conditions for the probe and pump beams, parallel ($S_{\parallel}$) and perpendicular ($S_{\perp}$).[38] We used a homemade cell of 25 μm path length consisting of two $CaF_2$ windows of 3 mm thickness and a Teflon spacer. Population relaxation, $P(t)$, (vibrational lifetime), was calculated using the following equation:

$$P(t) = (S_{\parallel} + S_{\perp})/3 \quad (1)$$

### D. 2D-IR vibrational echo spectroscopy

A mid-IR pulse centered at 2110 or 2060 cm$^{-1}$ was split into three pulses of approximately the same power. These three beams were focused onto the sample in BoxCARS geometry. Beam 3 ($k_3$) was fixed in time and chopped at 500 Hz. In 2D-IR vibrational echo spectroscopy, the temporal overlap of the three pulses leads to the generation of a third-order echo signal in the phase-matched direction ($-k_1 + k_2 + k_3$). This signal is heterodyne-detected by overlapping with a local oscillator. A monochromator dispersed the combined beam onto a 32-element MCT array detector ($\sim$2 cm$^{-1}$ per pixel resolution). We denote the times between beam 1 and beam 2, and between beam 2 and beam 3, as $\tau$ and $T_w$, respectively. The 2D-IR spectra were obtained as a function of $T_w$.

## Results and discussion

### A. FT-IR spectra of the azide probes

We measured the FT-IR spectra of the azide derivatives in DMF (Fig. 1). DMF was selected as a solvent due to the lack of protic hydrogens that can bring undesired complexity into the FT-IR spectrum by making a hydrogen bond with the azide group.

The azido stretch mode has a frequency of 2103.0 cm$^{-1}$ (Ala-$N_3$), and its spectrum exhibits the extended wing toward the high-frequency side as shown in Fig. 1(a). This asymmetric lineshape can be explained with the overlap of two spectral components centered at 2103.0 and 2127.0 cm$^{-1}$ (the detailed fitting results can be found in Table 1). The high-frequency peak is not visible in the spectrum without fitting because of its low intensity as well as much broader linewidth (70.7 cm$^{-1}$) compared to that of the main low-frequency peak with a linewidth of 25.5 cm$^{-1}$. Although such an asymmetric lineshape with a weak shoulder band has been observed in many FT-IR studies using azide as an IR probe, its assignment has not been clearly made yet. A few possibilities could be considered. Firstly, it could originate from different conformers with slightly different structures and solvation environments. Secondly, the error in the background solvent subtraction may produce the uneven baseline because the spectrum of the blank cell filled with solvent and buffer sometimes differs from that of the protein solution due to the change in the solvation structure. A certain number of solvent and buffer molecules are excluded from the light–matter interaction volume due to the occupation of proteins. Also, solvent–protein or buffer–protein interactions could affect the spectrum so that the solvent background spectra with and without proteins are different from each other. Thus, one needs to interpret the small peaks after background subtraction cautiously. Finally, there is a chance of Fermi resonance, which increases the complexity of the vibrational spectrum by introducing a shoulder peak or overlapping band in the FT-IR spectra due to anharmonic couplings between fundamental vibrations and overtones or combination bands of other modes. Usually, those overtone and combination bands are silent in the FT-IR spectrum because their transition dipoles are much smaller than that of the fundamental transition. However, when the frequency difference gets smaller, the Fermi resonance-enhanced overtone or combination bands appear in the spectrum, which makes the assignment of FT-IR peaks difficult.

Table 1 Fitting results for FT-IR spectra of azide derivatives in DMF (Fig. 1)

| | | Ala-$N_3$ | Ala-$N^{15}NN$ |
|---|---|---|---|
| Peak 1 | $\omega_{00}$ (cm$^{-1}$) | 2103.0 | 2062.0 |
| | FWHM (cm$^{-1}$) | 25.5 | 22.9 |
| | Area | 28.4 | 20.5 |
| Peak 2 | $\omega_0$ (cm$^{-1}$) | 2127.0 | |
| | FWHM (cm$^{-1}$) | 70.7 | |
| | Area | 7.9 | |

One of the useful methods to avoid Fermi resonance is through isotope labelling because it does not perturb the structure but just shifts the vibrational frequency of the fundamental transition significantly. As a result of the increased energy difference, the fundamental vibrational transition and other overtone or combination transitions become decoupled, and the Fermi resonance effect disappears or is significantly reduced. Here, we applied isotopic labelling to azide where one of the N atoms is labeled with heavy isotope $^{15}$N. In this study, we selectively labeled the β-position of the mid-N atom of azide group because a larger peak-shift is expected than other positions.[37] If the origin of the shoulder peak is Fermi resonance, the shoulder peak must disappear upon isotope labelling. Fig. 1 shows the FT-IR spectrum of Ala-$N^{15}NN$, which shows an absorption band fitted well with a single Voigt function centered at 2062.0 cm$^{-1}$. We have also measured the FT-IR spectra of both unlabeled and labeled azide in water as well to understand how the vibrational property gets changed depending upon the nature of the solvent.

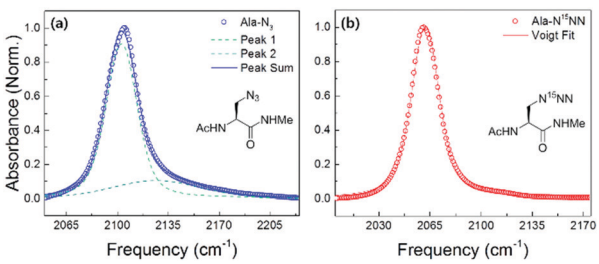


Fig. 1 Structures and Fourier-transformed infrared (FT-IR) spectra of (a) Ala-$N_3$ and (b) Ala-$N^{15}NN$ in DMF.

The fitting of the spectra of azide in water using the Voigt function is shown in Fig. S2 (ESI†), and the fitting parameters are tabulated in Table S2 of the ESI.† The asymmetric spectral shape of unlabeled azide and the symmetric line shape of the labeled azide in water indicates that the azide behaves similarly in water as compared to the DMF due to isotope substitution. Based on these results, the origin of the shoulder peak is believed to be Fermi resonance. Even though the isotope labelling is an efficient way to check the origin of small side peak, it requires additional synthetic procedures with cost and time.

### B. 2D-IR spectroscopy of the azide probes

2D-IR spectroscopy even without employing isotope labelling provides direct evidence on the existence of Fermi resonance band through the appearance of the cross-peaks. In fact, 2D-IR spectroscopy has been implemented on numerous occasions to find correlations between vibrational modes observed in various steady-state FT-IR spectra. Although a careful analysis of the 2D-IR spectrum can reveal the Fermi resonance directly,[39–42] the previous 2D-IR study mainly focused on the model system showing much stronger Fermi Resonance peak. When the two peaks have nearly the same intensity due to strong mixing of the transition dipoles, a cross-peak from the vibrational coupling appears at an early waiting time. However, no 2D-IR spectroscopic study for elucidating the origin of very weak spectral features, which have been frequently observed in many azido-IR spectroscopic studies of biological systems, has reported before.

Fig. 2 shows the 2D-IR vibrational echo spectra of the azido-derivatized alanine Ala-$N_3$ at $T_w$ = 0 ps. The 2D-IR spectrum consists of a positive peak originating from ground-state bleach and stimulated emission (Fig. 2; red) and a negative peak from excited-state absorption (Fig. 2; blue). The negative peak is red-shifted from the positive conjugate peak due to anharmonic shift, which is about 30 $cm^{-1}$ in the case of the azido stretch mode.

The 2D-IR spectrum of the Ala-$N_3$ (Fig. 2(a)) shows an indication of cross-peaks, but they are not clearly discernible. To confirm the existence of cross-peaks, we examined the 1D slice spectrum along the $\omega_\tau$ axis at the $\omega_m$ frequency indicated as a dotted line in each 2D-IR spectrum. Fig. 3 compares the FT-IR spectrum and the 1D slice spectrum obtained from the 2D-IR spectrum to emphasize the increased spectral resolution of 2D-IR from the spectral narrowing effect. As a result, the spectral feature of the hidden Fermi resonance peak becomes more apparent as a shoulder peak rather than the extended wing structure.

In addition to the spectral narrowing effect, it should be emphasized that the observation of cross-peak is possible because it borrows transition dipole strength from the strong fundamental absorption. As stated above, in a weak coupling case, there is a very small increase in transition dipole strength due to small mixing between strong fundamental transition and weak overtone/combination transitions. In 2D-IR spectrum, the intensity of cross-peak is proportional to the product $|\mu_A|^2 \times |\mu_F|^2$ where $\mu_A$ is the transition dipole of azide stretching band and $\mu_F$ is that of Fermi resonance peak. Since we have $\mu_A \gg \mu_F$, the intensities of two diagonal peaks and a cross-peak have the following order, $|\mu_A|^4 \gg |\mu_A|^2 \times |\mu_F|^2 \gg |\mu_F|^4$. Thus, even if the diagonal peak from Fermi resonance is not observed, the cross-peak can appear. Furthermore, the inhomogeneity produces the diagonally elongated spectrum along the diagonal line, which will overlap with a small diagonal peak from Fermi Resonance at early waiting times. The slice spectrum obtained along the diagonal line is also presented in Fig. 3(a) to show that there is no detectable feature from Fermi resonance in a diagonal line.

Ala-$N_3$ has a shoulder peak at a high frequency (Fig. 3(a)). After isotope labelling, the shoulder peak disappears like that in the FT-IR spectrum (Fig. 3(b)). The disappearance of the shoulder peak suggests that Fermi resonance is present in Ala-$N_3$, but due to the significant difference in intensity, no noticeable diagonal peaks are observed.

These complex absorption profiles of azide probes make them less attractive for use in 2D-IR and other linear IR spectroscopies. Firstly, the cross-peak and additional diagonal peaks substantially overlap with the diagonal peak from the fundamental mode, which complicates the analysis of the evolution of peak shape and spectral diffusion dynamics obtained from the diagonal peak. However, in the case of azido stretch mode of Ala-$N_3$, the center line slope (CLS) analysis may not be significantly affected due to the large transition dipole difference between the azido stretch mode and the combination modes participating in Fermi resonance. Secondly, due to coupling with the combination modes, the advantage as a local probe is lost. The IR probe is mostly sensitive to the local solvation structure directly interating with IR probe. However, Fermi

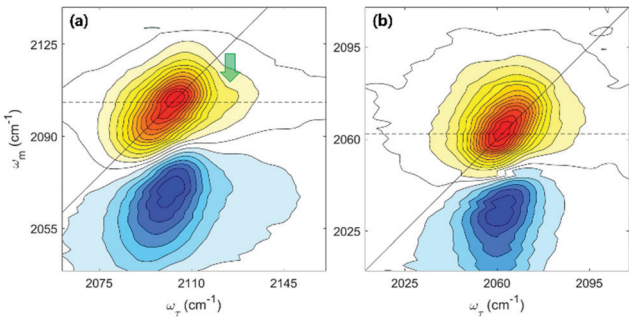


Fig. 2 2D-infrared (IR) vibrational echo spectra for (a) Ala-$N_3$ and (b) Ala-$N^{15}NN$ in DMF at zero waiting time ($T_w$ = 0 ps).

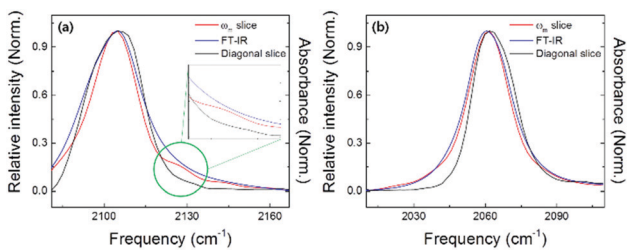


Fig. 3 Normalized Fourier-transform (FT-IR) spectra, 1D slices of 2D spectra, and diagonal slices of 2D spectra of (a) Ala-$N_3$ and (b) Ala-$N^{15}NN$ in DMF. 1D slices along $\omega_\tau$ at: (a) $\omega_m$ = 2103 and (b) 2062 $cm^{-1}$. To illustrate the locations of the 1D slices, dashed lines are shown in the 2D spectra (Fig. 2).

resonance couples the vibrational mode of IR probe to the combination/overtone band where many atoms in the molecule often participate. Thus, structural and solvational changes in remote site from IR probe can affect the spectral properties of IR probe group. Lastly, Fermi resonance provides faster vibrational energy relaxation pathways through anharmonic coupling with combination or overtone bands, which significantly reduce the vibrational lifetime of the probe. As shown in Fig. 2(b) and 3(b), isotope-labeled azides simplified the spectral feature and enhanced spectral sensitivity from the conformational change or solvation fluctuations. To find out the origin of the weak Fermi resonance band and to ensure that the isotope labeling does not impact the near-resonant bands participated in the Fermi resonance, the anharmonic frequency analysis has been performed, which are presented in detail in the 'anharmonic frequency analysis' section of the ESI.† It can be observed from the Tables S3, S4, and Fig. S3 of the ESI,† that two combination bands consist of normal modes 30 & 39, and 28 & 41 can participate in the Fermi resonance with the azide asymmetric stretch mode. All these bands mainly consist of $N_3$ symmetric stretch, CN stretch, $CH_2$ bend, chain C–H bend, and N–H bend vibrations, as depicted in Fig. S3 (ESI†), but none of them consists the isotope labeled N atom of the azide. Thus, it can be concluded from this anharmonic frequency analysis that the $^{15}N$ substitution to middle N atom of the $-N_3$ does not impact other near-resonant combination bands, which asserts the strategy of incorporating $^{15}N$ to azide group as an effective means to remove Fermi resonance from the spectra.

### C. IR pump–probe spectroscopy of the azide probes

Further, we explored the isotope labelling effects on the vibrational lifetimes of the aliphatic azides *via* polarization-controlled IR pump–probe experiments. In addition to the absorption frequency of the IR probe, the vibrational dynamics is expected to be affected by isotope labelling. IR probes are designed for *in vivo* studies of transient molecular structural changes, such as those occurring in proteins and DNA. The time-scale of protein dynamics reported by 2D-IR spectroscopy is limited by the vibrational lifetimes of the IR probes, which are typically within a few picoseconds.[43]

This issue spurred us to develop IR probes with longer lifetimes involving –SCN, –SeCN, and –NC functionalized amino acids.[44–47] Rodgers *et al.* studied CN isotopomers of Phe-CN as IR probes. They found a longer vibrational lifetime ($7.9 \pm 0.5$ ps) for Phe-$^{13}C^{15}N$ upon isotope labelling, making it more useful than Phe-CN ($4.0 \pm 0.2$ ps) in real-time applications.[48] A typical IR pump–probe spectrum consists of a positive peak in the high-frequency side and a negative peak on the low-frequency side. The positive peak arises from ground-state bleaching (GSB) and stimulated emission (SE), while the negative peak originates from excited-state absorption (ESA). We refer to a positive peak as a 0–1 transition and a negative peak as a 1–2 transition.

In Fig. 4, we show the pump–probe decay profiles of the 1–2 transitions of both the (a) Ala-$N_3$ and (b) Ala-$N^{15}NN$ before and after isotope labelling. For the excited-state decay kinetics, we expected that there would be a coherent oscillation feature in the Ala-$N_3$, which should exist because of the Fermi resonance.[40,41]

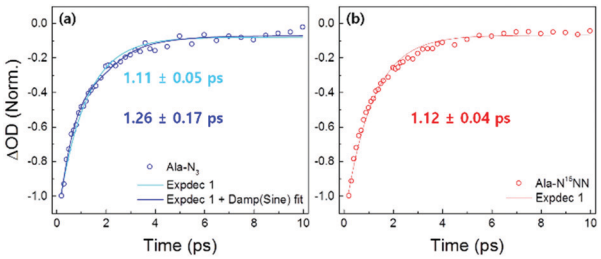


Fig. 4 1–2 transition decay of (a) Ala-$N_3$ and (b) Ala-$N^{15}NN$ in DMF. The smooth line for Ala-$N_3$ is fitting curves containing both mono-exponential decay (cyan) and mono-exponential decay and damped sine components (blue). The smooth line for Ala-$N^{15}NN$ corresponds to a mono-exponential decay function. Selected probe frequencies: 2074 $cm^{-1}$ for Ala-$N_3$, 2034 $cm^{-1}$ for Ala-$N^{15}NN$. The vibrational lifetime of Ala-$N_3$ was determined to be $1.11 \pm 0.05$ ps for the fitting using mono-exponential decay and $1.26 \pm 0.13$ ps for mono-exponential and damped oscillation, respectively. The vibrational lifetime of Ala-$N_3$ was determined to be $1.26 \pm 0.13$ ps.

Thus, we fitted with mono-exponential function with damped oscillation for Ala-$N_3$ (Fig. S1 and Table S1, ESI†). The exponential decay constant or vibrational lifetime of Ala-$N_3$ was determined to be $1.26 \pm 0.17$ ps. As shown in Fig. 4(a), however, the pump–probe signal does not produce a clear, coherent oscillation. For comparison, we also used a mono-exponential decay function and obtained the decay time constant as $1.11 \pm 0.05$ ps. Although the change in a vibrational lifetime was not large, the analysis using the damped sine function is more accurate because it fits better than mono-exponential function without the damped sine function, especially around 2–4 ps range (Fig. S1(b), ESI†). As we can understand from the FT-IR spectra, 2D-IR spectra at zero waiting time, and its 1D slice that the Fermi resonance appears from the weakly coupled state, the contribution from the oscillatory part in the vibrational relaxation dynamics is very little in Ala-$N_3$. This observation explains why the lifetime of the azide stretch mode using two different models, namely exponential and oscillatory decay, does not change much. Conversely, Ala-$N^{15}NN$ is well fit by a mono-exponential decay function (Fig. 4(b)).

We observe that the periods of the oscillatory beating response of the Ala-$N_3$ (Fig. 4(a)) is $\approx$1.39 ps, which are consistent with the energy gap between the two vibrational transitions 24 $cm^{-1}$. We tentatively assign the oscillatory response of the decay profiles to the coherent excitation of Fermi-coupled states. The vibrational lifetime of the asymmetric stretch mode of Ala-$N_3$ was determined to be $1.26 \pm 0.13$ ps in comparison to $1.12 \pm 0.04$ ps in the case of Ala-$N^{15}NN$ in DMF. Therefore, the vibrational lifetime of the aliphatic azide slightly decreases due to isotope labelling, but the difference was not significantly changed. When the existing Fermi resonance was strongly observed, it was found that the oscillatory component was prominent even in the IR pump–probe spectra.[40] Because the Fermi resonance is present as a weak coupling, it is difficult to distinguish the origin of small side peaks with the IR pump–probe spectra alone. This study reveals that the vibrational relaxation of the aliphatic azide does not slow down despite the selective isotope labelling at the mid-N atom. Also, compared to

the less pronounced oscillatory component in IR pump–probe spectrum, the hidden Fermi resonance can be identified more clearly from the 2D-IR spectrum.

## Conclusions

This study suggests that Fermi resonance could also exist through weak coupling in the aliphatic azide, which cause uncertainty when observing the structural and dynamical changes of the protein by using such an aliphatic azide-based IR probe. Therefore, the present work demonstrates that it is desirable to investigate the effect of isotope labelling in aliphatic azide-based IR probes, even if it is expensive in terms of time-consuming synthetic procedures and cost.

Detailed analyses of cross peak in the 2D-IR spectrum revealed that the origin of the azide stretch shoulder peak is indeed a Fermi resonance band even though it is almost hidden under the tail part of the azide stretch IR spectrum. Azide is one of the frequently used IR probes due to its strong dipole strength compared to other IR probes. Thus, the detailed knowledge of the spectral signature of azide is essential to correctly interpret the spectral change induced by the structural and environmental variations of the protein.

What differentiates the present work from the previous works? Fermi resonance bands have been studied for aromatic azide derivatives because the anharmonic coupling is very strong in those cases. For instance, the Brewer group clearly demonstrated that such a strong Fermi resonance band can be removed by introducing an $^{15}$N-isotope into the middle of azide group of 3-azidopyridine, which makes the corresponding IR absorption spectrum a singlet.[37] However, substantially detailed FTIR and 2D-IR spectroscopic investigations of azdo-alanine and its isotope-labeled analog have not been performed before. As shown here, the 1D slice spectrum obtained from the 2D-IR spectrum exhibits a notable signature of a weak Fermi resonance band.

Furthermore, even though 2D-IR was used to study the details of Fermi resonance phenomena in azido-derivatized compounds, it has been applied only to model compounds with strong couplings. Because time-resolved IR spectroscopic techniques have been increasingly applied to a wide variety of complex biological systems, it becomes necessary to elucidate subtle spectral and transient changes of time-dependent signals. Thereby, the use of site-specific local IR probes, which are disconnected from other vibrational motions will gain popularity. We believe that the 2D-IR study about the spectral feature of the IR probe will help to develop an ideal IR probe.

## Conflicts of interest

There are no conflicts to declare.

## Acknowledgements

This work was supported by the Institute for Basic Science (IBS-R023-D1). H. H. is grateful for the financial support from the National Research Foundation (NRF) of Korea funded by the Ministry of Science and ICT (NRF2020R1F1A1049520).

## References

1 B. A. Griffin, S. R. Adams and R. Y. Tsien, *Science*, 1998, **281**, 269–272.
2 B. N. G. Giepmans, S. R. Adams, M. H. Ellisman and R. Y. Tsien, *Science*, 2006, **312**, 217–224.
3 A. Miyawaki, J. Llopis, R. Heim, J. M. McCaffery, J. A. Adams, M. Ikura and R. Y. Tsien, *Nature*, 1997, **388**, 882–887.
4 R. Y. Tsien, *Annu. Rev. Biochem.*, 1998, **67**, 504–544.
5 A. Chattopadhyay and S. G. Boxer, *J. Am. Chem. Soc.*, 1995, **117**, 1449–1450.
6 E. S. Park and S. G. Boxer, *J. Phys. Chem. B*, 2002, **106**, 5800–5806.
7 A. T. Fafarman, L. J. Webb, J. I. Chuang and S. G. Boxer, *J. Am. Chem. Soc.*, 2006, **128**, 13356–13357.
8 K.-I. Oh, J.-H. Lee, C. Joo, H. Han and M. Cho, *J. Phys. Chem. B*, 2008, **112**, 10352–10357.
9 R. Adhikary, J. Zimmermann and F. E. Romesberg, *Chem. Rev.*, 2017, **117**, 1927–1969.
10 J.-H. Choi, K.-I. Oh and M. Cho, *J. Chem. Phys.*, 2008, **129**, 174512.
11 J.-H. Choi, D. Raleigh and M. Cho, *J. Phys. Chem. Lett.*, 2011, **2**, 2158–2162.
12 X. S. Gai, B. A. Coutifaris, S. H. Brewer and E. E. Fenlon, *Phys. Chem. Chem. Phys.*, 2011, **13**, 5926–5930.
13 K.-K. Lee, K.-H. Park, C. Joo, H.-J. Kwon, J. Jeon, H.-I. Jung, S. Park, H. Han and M. Cho, *J. Phys. Chem. B*, 2012, **116**, 5097–5110.
14 K.-K. Lee, K.-H. Park, C. Joo, H.-J. Kwon, H. Han, J.-H. Ha, S. Park and M. Cho, *Chem. Phys.*, 2012, **396**, 23–29.
15 M. P. Wolfshorndl, R. Baskin, I. Dhawan and C. H. Londergan, *J. Phys. Chem. B*, 2012, **116**, 1172–1179.
16 C. G. Bazewicz, M. T. Liskov, K. J. Hines and S. H. Brewer, *J. Phys. Chem. B*, 2013, **117**, 8987–8993.
17 H. Taskent-Sezgin, J. Chung, P. S. Banerjee, S. Nagarajan, R. B. Dyer, I. Carrico and D. P. Raleigh, *Angew. Chem., Int. Ed.*, 2010, **49**, 7473–7475.
18 R. Bloem, K. Koziol, S. A. Waldauer, B. Buchli, R. Walser, B. Samatanga, I. Jelesarov and P. Hamm, *J. Phys. Chem. B*, 2012, **116**, 13705–13712.
19 R. Adhikary, J. Zimmermann, P. E. Dawson and F. E. Romesberg, *ChemPhysChem*, 2014, **15**, 849–853.
20 S. M. Decatur, *Acc. Chem. Res.*, 2006, **39**, 169–175.
21 S. H. Brewer, B. Song, D. P. Raleigh and R. B. Dyer, *Biochemistry*, 2007, **46**, 3279–3285.
22 A. T. Krummel and M. T. Zanni, *J. Phys. Chem. B*, 2008, **112**, 1336–1338.
23 S. Ye, E. Zaitseva, G. Caltabiano, G. F. Schertler, T. P. Sakmar, X. Deupi and R. Vogel, *Nature*, 2010, **464**, 1386–1389.
24 M. J. Tucker, X. S. Gai, E. E. Fenlon, S. H. Brewer and R. M. Hochstrasser, *Phys. Chem. Chem. Phys.*, 2011, **13**, 2237–2241.

 

25 C. G. Bazewicz, J. S. Lipkin, E. E. Smith, M. T. Liskov and S. H. Brewer, *J. Phys. Chem. B*, 2012, **116**, 10824–10831.
26 M. M. Waegele, R. M. Culik and F. Gai, *J. Phys. Chem. Lett.*, 2011, **2**, 2598–2609.
27 A. L. L. Sueur, R. E. Horness and M. C. Thielges, *Analyst*, 2015, **140**, 4336–4349.
28 A. Ghosh, J. S. Ostrander and M. T. Zanni, *Chem. Rev.*, 2017, **117**, 10726–10759.
29 Z. Ganim, H. S. Chung, A. W. Smith, L. P. Deflores, K. C. Jones and A. Tokmakoff, *Acc. Chem. Res.*, 2008, **41**, 432–441.
30 J. R. Hill, A. Tokmakoff, K. A. Peterson, B. Sauter, D. Zimdars, D. D. Dlott and M. D. Fayer, *J. Phys. Chem.*, 1994, **98**, 11213–11219.
31 A. Xie, L. v. D. Meer, W. Hoff and R. H. Austin, *Phys. Rev. Lett.*, 2000, **84**, 5435–5438.
32 H. Maekawa, C. Toniolo, A. Moretto, Q. B. Broxterman and N. H. Ge, *J. Phys. Chem. B*, 2006, **110**, 5834–5837.
33 D. C. Urbanek, D. Y. Vorobyev, A. L. Serrano, F. Gai and R. M. Hochstrasser, *J. Phys. Chem. Lett.*, 2010, **1**, 3311–3315.
34 A. L. Serrano, M. M. Waegele and F. Gai, *Protein Sci.*, 2012, **21**, 157–170.
35 M. J. Tucker, Y. S. Kim and R. M. Hochstrasser, *Chem. Phys. Lett.*, 2009, **470**, 80–84.
36 M. Okuda, K. Ohta and K. Tominaga, *J. Chem. Phys.*, 2015, **142**, 212418.
37 J. S. Lipkin, R. Song, E. E. Fenlon and S. H. Brewer, *J. Phys. Chem. Lett.*, 2011, 1672–1676.
38 H. Tan, I. R. Piletic and M. D. Fayer, *J. Opt. Soc. Am. B*, 2005, **22**, 2009–2017.
39 M. W. Nydegger, S. Dutta and C. M. Cheatum, *J. Chem. Phys.*, 2010, **133**, 134506.
40 J. M. Rodgers, R. M. Abaskharon, B. Ding, J. Chen, W. Zhang and F. Gai, *Phys. Chem. Chem. Phys.*, 2017, **19**, 16144–16150.
41 J. Zhang, L. Wang, J. Zhang, J. Zhu, X. Pan, Z. Cui, J. Wang, W. Fang and Y. Li, *J. Phys. Chem. B*, 2018, **122**, 8122–8133.
42 J. Edler and P. Hamm, *J. Chem. Phys.*, 2003, **119**, 2709–2715.
43 Z. Getahun, C. Y. Huang, T. Wang, B. D. León, W. F. DeGrado and F. Gai, *J. Am. Chem. Soc.*, 2003, **125**, 405–411.
44 S. Ramos, K. J. Scott, R. E. Horness, A. L. L. Sueur and M. C. Thielges, *Phys. Chem. Chem. Phys.*, 2017, **19**, 10081–10086.
45 K.-H. Park, J. Jeon, Y. Park, S. Lee, H.-J. Kwon, C. Joo, S. Park, H. Han and M. Cho, *J. Phys. Chem. Lett.*, 2013, **4**, 2105–2110.
46 D. E. Levin, A. J. Schmitz, S. M. Hines, K. J. Hines, M. J. Tucker, S. H. Brewer and E. E. Fenlon, *RSC Adv.*, 2016, **43**, 36231–36237.
47 M. Maj, C. Ahn, D. Kossowska, K. Park, K. Kwak, H. Han and M. Cho, *Phys. Chem. Chem. Phys.*, 2015, **17**, 11770–11778.
48 J. M. Rodgers, W. Zhang, C. G. Bazewicz, J. Chen, S. H. Brewer and F. Gai, *J. Phys. Chem. Lett.*, 2016, **7**, 1281–1287.